Constraining nucleon high momentum in nuclei

Gao-Chan Yong
Institute of Modern Physics, Chinese Academy of Sciences, Lanzhou 730000, China

Recent studies at Jefferson Lab show that there are a certain proportion of nucleons in nuclei have momenta greater than the so-called nuclear Fermi momentum p_F. Based on the transport model of nucleus-nucleus collisions at intermediate energies, nucleon high momentum caused by the neutron-proton short-range correlations in nuclei is constrained by comparing with π and photon experimental data and considering some uncertainties. The high momentum cutoff value $p_{max} \leq 2p_F$ is obtained.

PACS numbers: 25.70.-z

The picture of nucleons have maximal momentum — so called the Fermi momentum p_F — in a nuclear system and roughly move independently in the mean field created by their mutually attractive interactions has been established since the 1950s. However, recent proton-removal experiments using electron beams with energies of several hundred MeV showed that only about 80% nucleons participate in this type of independent particle motion [1–3]. And high-momentum transfer measurements have shown that nucleons in nuclei can form pairs with larger relative momenta and smaller center-of-mass momenta [4, 5]. This is interpreted by the nucleon-nucleon tensor interaction in short range [6, 7]. The nucleon-nucleon short-range correlations (SRC) in nuclei leads to a high-momentum tail in single-nucleon momentum distribution above 300 MeV/c [8–12]. And interestingly, the high-momentum tail's shape caused by two-nucleon SRC is almost identical for all nuclei from deuteron to very heavier nuclei [13–16], i.e., roughly exhibits a C/k^4 tail [17–20]. Nucleon momentum distributions at even higher momenta are due to three or many-nucleon correlations. This part of momentum-distribution probability was deduced to be less than 1% [21]. We thus in this study neglect this kind of high-momentum nucleons caused by many-nucleon short-range correlations.

In the high-momentum tail (HMT) of nucleon momentum distribution, nucleon component is strongly isospin-dependent, i.e., the number of n-p SRC pairs is about 18 times that of the p-p or n-n SRC pairs [3], thus in neutron-rich heavy nuclei proton has greater probability than neutron to have momenta greater than the nuclear Fermi momentum [20]. In neutron stars, the number of protons only has a small proportion. The above n-p SRC in neutron stars will cause proton average kinetic energy far greater than neutron's [22]. And the stronger the n-p SRC is, the larger the difference of proton and neutron average kinetic energy is seen.

Nucleon spectral function provides fundamental information on the dynamics of nucleon in nuclear medium. The nuclear momentum distribution can be obtained from the spectral function by integrating over the excitation energy [13, 23]. The high-momentum nucleons come predominantly from the high excitation energy regime of the spectral function. The high-momentum cutoff parameter λ ($= p_{max}/p_F$, i.e., the ratio of nucleon maximal momentum over the nuclear Fermi momentum) was first introduced by *Hen et al.* as a free parameter in the Correlated Fermi Gas model — an analytical approximation for the momentum distribution of nucleon in symmetric nuclei and nuclear matter [18], to avoid divergence when calculating nucleon average kinetic energy assuming a C/k^4 dependence for the high-momentum tail. Therefore, the implication of the value of this *effective* parameter λ is the determination of the average kinetic energy of nucleons.

The value of average kinetic energy of nucleons and the high-momentum tail of nucleon distribution in nuclei surely affect the yields of π, K, η and nucleon emission in heavy-ion collisions at intermediate energies. The isospin dependence of nucleon high-momentum distribution definitely affects transport calculations of the symmetry-energy sensitive observables. More specifically, a low (high) value of average kinetic energy of nucleons causes a small (large) number of meson production in transport calculations owing to low (high) value of collision energy of nucleon pairs. Because in neutron-rich heavy nuclei protons have greater probability than neutrons to have momenta greater than the nuclear Fermi momentum, the high-momentum tail of nucleon momentum distribution affects values of π^-/π^+ ratio and the difference of neutron and proton elliptic flows [24]. Values of average kinetic energy of neutrons and protons in nuclei also strongly affect nuclear kinetic symmetry energy [18, 19], the latter is known plays crucial role in both nuclear physics and astrophysics [25].

In fact, one can deduce the high-momentum cutoff parameter λ from nucleon momentum distribution in deuteron [17, 18] or from the high-energy electron scattering measurements [20, 21]. But the high-energy electron scattering measurements mainly probe the nucleon momenta at the surface of nuclei [26]. Since the production of π^+ meson in nucleus-nucleus collisions at intermediate energies is mainly from proton-proton collision [27], and energetic neutron-proton scattering produces hard bremsstrahlung photon [28–30], the high momentum of nucleon in projectile or target should affect π^+ and hard photon productions. In this study, we use hadronic probe π^+ meson and electromagnetic probe hard photon in nucleus-nucleus collisions to probe nucleon high-momentum cutoff value.

To obtain the high-momentum cutoff value of nucleon in nuclei by nucleus-nucleus collisions, we use the Boltzmann-Uehling-Uhlenbeck (BUU) transport model [31], which has been very successful in studying heavy-ion collisions at intermediate energies. The BUU transport model describes time evolution of the single particle phase space distribution function $f(\vec{r},\vec{p},t)$, which reads

$$\frac{\partial f}{\partial t}+\nabla_{\vec{p}}E\cdot\nabla_{\vec{r}}f-\nabla_{\vec{r}}E\cdot\nabla_{\vec{p}}f=I_c. \quad (1)$$

The phase space distribution function $f(\vec{r},\vec{p},t)$ denotes the probability of finding a particle at time t with momentum $\vec{p}$ at position $\vec{r}$. The left-hand side of Eq. (1) denotes the time evolution of the particle phase space distribution function due to its transport and mean field, and the right-hand side collision item I_c accounts for the modification of phase space distribution function by elastic and inelastic two body collisions [31–33]. E is a particle's total energy, which is equal to kinetic energy E_{kin} plus its average potential energy U. While the mean-field potential U of single particle depends on its position and momentum of the particle and is given self-consistently by its phase space distribution function $f(\vec{r},\vec{p},t)$.

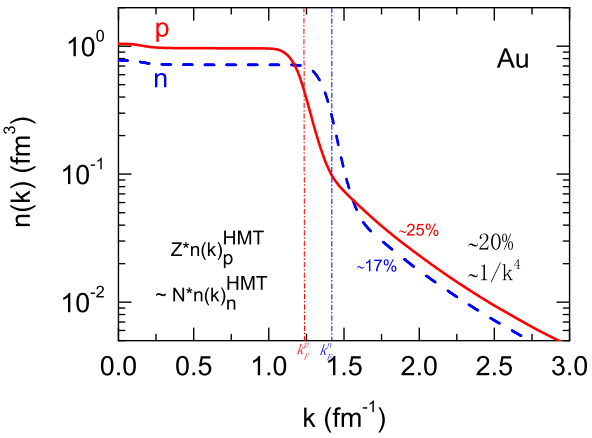

FIG. 1: (Color online) Momentum distribution n(k) of neutron and proton in nucleus $^{197}_{79}Au$ with normalization condition $4\pi\int_0^{\lambda k_F^{p,n}} n_{p,n}(k)k^2dk=1$ as well as $4\pi\int_{k_F^p}^{\lambda k_F^p} n_p(k)k^2dk \simeq 25\%$ and $4\pi\int_{k_F^n}^{\lambda k_F^n} n_n(k)k^2dk \simeq 17\%$.

In the used BUU model, nucleon spatial distribution in initial colliding nuclei is given by [31]

$$r=R(x_1)^{1/3}; cos\theta=1-2x_2; \phi=2\pi x_3. \quad (2)$$

$$x=rsin\theta cos\phi; y=rsin\theta sin\phi; z=rcos\theta. \quad (3)$$

Where R is the radius of nuclei, x_1, x_2, x_3 are three independent random numbers. Since there is a rough 20% depletion of nucleon momentum distribution inside the Fermi sea [3, 11, 20, 34, 35], we let nucleon momentum distributions in the high-momentum tail $n^{HMT}(k)\sim 1/k^4$ [17] and $\int_{k_F}^{\lambda k_F} n^{HMT}(k)k^2dk/\int_0^{\lambda k_F} n(k)k^2dk \simeq 20\%$ and keeping $n_p^{HMT}(k)/n_n^{HMT}(k)\simeq N/Z$ (N and Z being the neutron and proton numbers of a nucleus) [3, 20, 34]. As shown in Fig. 1, there are about 25% (17%) protons (neutrons) with momenta larger than the proton (neutron) Fermi momentum. With this nucleon momentum distribution, the average kinetic energy of nucleons in this study increases roughly several MeV comparing to that with ideal Fermi-Gas model. We thus neglect this difference in heavy-ion collisions at 400 MeV/nucleon beam energy.

In this model, an isospin- and momentum-dependent mean-field single nucleon potential is used [36, 37], which reads

$$\begin{aligned} U(\rho,\delta,\vec{p},\tau) &= A_u(x)\frac{\rho_{\tau'}}{\rho_0}+A_l(x)\frac{\rho_\tau}{\rho_0} \\ &+B(\frac{\rho}{\rho_0})^\sigma(1-x\delta^2)-8x\tau\frac{B}{\sigma+1}\frac{\rho^{\sigma-1}}{\rho_0^\sigma}\delta\rho_{\tau'} \\ &+\frac{2C_{\tau,\tau}}{\rho_0}\int d^3\vec{p'}\frac{f_\tau(\vec{r},\vec{p'})}{1+(\vec{p}-\vec{p'})^2/\Lambda^2} \\ &+\frac{2C_{\tau,\tau'}}{\rho_0}\int d^3\vec{p'}\frac{f_{\tau'}(\vec{r},\vec{p'})}{1+(\vec{p}-\vec{p'})^2/\Lambda^2}, \end{aligned} \quad (4)$$

where $\tau,\tau'=1/2(-1/2)$ for neutrons (protons), $\delta=(\rho_n-\rho_p)/(\rho_n+\rho_p)$ is the isospin asymmetry, and ρ_n, ρ_p denote neutron and proton densities, respectively. The parameter values $A_u(x)$ = 33.037 - 125.34x MeV, $A_l(x)$ = -166.963 + 125.34x MeV, B = 141.96 MeV, $C_{\tau,\tau}$ = 18.177 MeV, $C_{\tau,\tau'}$ = -178.365 MeV, σ = 1.265, and Λ = 630.24 MeV/c are obtained by fitting empirical constraints of the saturation density ρ_0 = 0.16 fm^{-3}, the binding energy E_0 = -16 MeV, the incompressibility K_0 = 230 MeV, the isoscalar effective mass $m_s^*=0.7m$, the single-particle potential U_∞^0 = 75 MeV at infinitely large nucleon momentum at saturation density in symmetric nuclear matter, the symmetry energy $S(\rho)$ = 30 MeV (we let kinetic symmetry energy roughly be 0 MeV [38]) and the symmetry potential U_∞^{sym} = -100 MeV at infinitely large nucleon momentum at saturation density. $f_\tau(\vec{r},\vec{p})$ is the phase-space distribution function at coordinate $\vec{r}$ and momentum $\vec{p}$ and solved by using the test-particle method numerically. Different symmetry energy's stiffness parameters x can be used in the above single nucleon potential to mimic different forms of the symmetry energy predicted by various many-body theories [39] without changing any property of the symmetric nuclear matter and the symmetry energy at normal density. In this study, however, both π^+ production in Au + Au collisions and hard photon production in C + C collisions are in fact not sensitive to the symmetry energy parameter x.

According to baryon effective mass, the isospin-dependent baryon-baryon (BB) scattering cross section

in medium σ_{BB}^{medium} is reduced compared with their free-space value σ_{BB}^{free} by a factor of [33]

$$R_{medium}(\rho,\delta,\vec{p}) \equiv \sigma_{BB}^{medium}/\sigma_{BB}^{free} = (\mu_{BB}^{*}/\mu_{BB})^2, \quad (5)$$

where μ_{BB} and μ_{BB}^{*} are the reduced masses of the colliding baryon-pair in free space and medium, respectively. This form of reduced elastic baryon-baryon scattering cross section in medium agrees well with our recent study [29]. Since the inelastic baryon-baryon scattering cross section in medium is less known but crucial for π production [40], we in the present model extend the above reduced factor $R_{medium}(\rho,\delta,\vec{p})$ to inelastic baryon-baryon scattering cross section [41]. Other treatments related to π production are similar to that in Ref. [42].

For hard photon production from neutron-proton bremsstrahlung, we use the prediction of the one boson exchange model by Gan et al. [28–30, 43]

$$p_\gamma \equiv \frac{dN}{d\varepsilon_\gamma} = 2.1\times10^{-6}\frac{(1-y^2)^\alpha}{y}, \quad (6)$$

where $y=\varepsilon_\gamma/E_{max}$, $\alpha = 0.7319 - 0.5898\beta_i$, ε_γ is energy of emitting photon, E_{max} is the energy available in the center of mass of the colliding proton-neutron pairs, β_i is the initial velocity of the proton in the proton-neutron center of mass frame. The pauli-blockings of final state scattering neutron and proton in $pn \to pn\gamma$ process are taken into account [44].

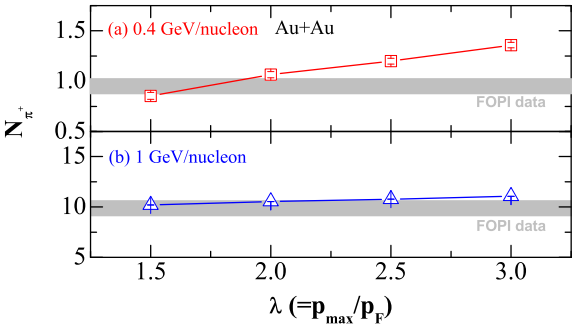

FIG. 2: (Color online) The number of produced π^+ meson as a function of high-momentum cutoff parameter λ in the Au + Au collisions at, respectively, 0.4 and 1 GeV/nucleon beam energies.

Fig. 2 shows π^+ production as a function of high-momentum cutoff parameter λ of colliding nuclei in the Au + Au collisions at 0.4 and 1 GeV/nucleon incident beam energies, respectively. One can clearly see that as the high-momentum cutoff parameter λ increases, more π^+'s are produced. Larger high-momentum cutoff parameter λ causes larger nucleon average kinetic energy, especially proton average kinetic energy [20], thus the average center-of-mass energy of proton-proton collision also becomes larger. As a consequence more π^+'s are produced in nucleus-nucleus collision [27]. This is the reason why one sees in the upper panel of Fig. 2 more π^+'s are produced with large high-momentum cutoff parameter λ. As incident beam energy increases, the initial movement of nucleons in nuclei becomes less important in nucleus-nucleus collisions. We thus see, in the lower panel of Fig. 2, at 1 GeV/nucleon incident beam energy, π^+ production is less sensitive to the high-momentum cutoff parameter λ (At 0.4 GeV/nucleon, the sensitivity of π^+ production to λ is about 10 times that of π^+ at 1 GeV/nucleon). Fig. 2 shows $\lambda \leq 2$ is favored by the FOPI data [45].

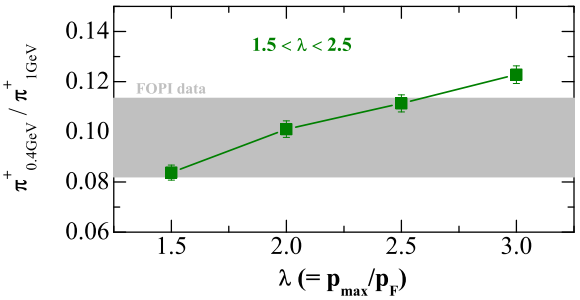

FIG. 3: (Color online) Constraints on the high-momentum cutoff parameter λ by the ratio of π^+ productions in the Au + Au collision at low and high beam energies. The shadow region denotes the FOPI data [45].

Since π^+ production is sensitive to the high-momentum cutoff parameter λ only at relative low beam energy, one can construct the ratio of π^+'s produced from low and high incident beam energies to probe the high-momentum cutoff parameter. This ratio is expected to reduce the system errors in some degree. Shown in Fig. 3 is the ratio of π^+ productions at 0.4 and 1 GeV/nucleon incident beam energies as a function of high-momentum cutoff parameter λ. As expected, the ratio of π^+ multiplicities produced respectively from low and high beam energies are still very sensitive to the high-momentum cutoff parameter λ. By comparison with the FOPI pion production data [45], a constraint of $1.5 \leq \lambda \leq 2.5$ is obtained. This result is surprisingly similar to that in Ref. [21].

The hadronic probe π^+ production inevitably suffers from distortions due to the strong interactions in the final state. Ideally one would like to have more clean ways to probe the high-momentum tail of nucleon in nucleus. Photons interact with nucleons only electromagnetically, once produced they escape almost freely from the nuclear environment in nuclear reactions. In this regard, we also use hard photon production to constrain the high-

momentum cutoff parameter λ.

Hard photon production in heavy-ion reactions at beam energies below 200 MeV/nucleon had been in fact extensively studied both experimentally and theoretically [28–31, 46–48]. The TAPS collaboration carried out a series of comprehensive measurements studying in detail the properties of hard photons [49–52]. Theoretically, it was concluded that the neutron-proton bremsstrahlungs in the early stage of the reaction are the main source of high energy γ rays [53, 54]. And it was demonstrated that the hard photons can be used to probe the reaction dynamics leading to the formation of dense matter [44, 55–58]. And effects of the nuclear Equation of State (EOS) on the hard photon production were found small [59]. Although the input elementary $pn \to pn\gamma$ probability is still model dependent [43, 60–63], the experimental data can be described reasonably well theoretically within a factor of 2 [48]. And the experimental efforts have the potential to improve the situation significantly in the near future [64].

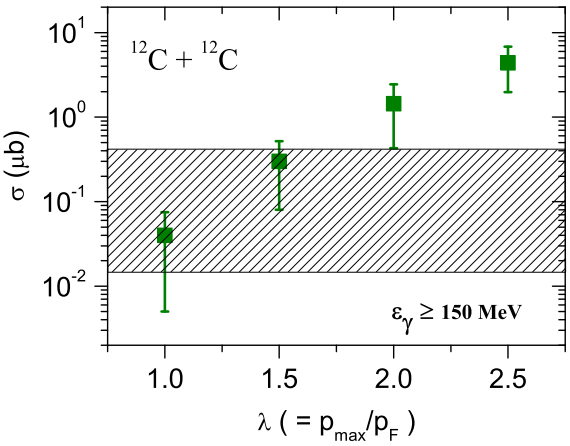

FIG. 4: (Color online) Inclusive photon production cross sections ($\varepsilon_\gamma \geq 150$ MeV) in ^{12}C+^{12}C collisions at the beam energy of 60 MeV/nucleon. The symbols stand for BUU calculations with, respectively, $\lambda = 1$ (i.e., without HMT), 1.5, 2, 2.5. The shadow region denotes experimental data [28, 46].

Fig. 4 shows comparison of theoretical inclusive hard photon production cross sections in ^{12}C+^{12}C collisions and the experimental data [28, 46]. Since the hadronic probe π^+ production constrained the high-momentum cutoff parameter λ between 1.5 $\sim$ 2.5, we use $\lambda = 1.5$, 2, 2.5 as the BUU calculations with the high-momentum tail. As comparison, we also calculated the case without high-momentum tail ($\lambda = 1$). From Fig. 4, it is seen that the hard photon production cross section in heavy-ion collisions is very sensitive to the HMT of nuclei [30]. The BUU calculations with $\lambda = 2$ and 2.5 are larger than the experimental hard photon production cross section. And the case of BUU calculation without HMT is somewhat lower than the experimental data. From Fig. 4, it is seen that the electromagnetic probe hard photon constrains the the high-momentum cutoff parameter to be $\lambda \leq 2$. Combining the constraints from hadronic probe π^+ production (shown in Fig. 3) and that from electromagnetic probe hard photon production (shown in Fig. 4), we can conservatively conclude that the value of the high-momentum cutoff parameter λ in nuclei is less than 2.5 and the overlap-area is $\lambda \leq 2$, which is smaller than that deduced in other lecture [17–19].

A small value of lambda implies lower average nucleon kinetic energy. The lower average nucleon kinetic energy implies smaller collision energy of nucleon pairs in transport calculations. This causes small number of meson production in heavy-ion collisions at low and intermediate energies. And it also cause smaller number of energetic nucleon or meson emissions, a high value of π^-/π^+ ratio [24] and small number of hard photon production in heavy-ion collisions at low and intermediate energies. A small value of lambda also implies a relatively larger nuclear kinetic symmetry energy, thus causes the reduction of nuclear symmetry potential [18]. The reduction of nuclear symmetry potential in heavy-ion collisions at intermediate energies decreases the sensitivity of isospin-sensitive observables.

Because the high-momentum tail of nucleon momentum distribution is in fact caused by the short-range correlations of nucleons, while in our transport model (besides nucleon-nucleon or nucleon-meson collisions and nuclear pauli-blockings) only a mean-field potential is used. Thus the nuclei in the evolution before collision may be instable. Lacking of the binding of high-momentum nucleons in nuclei, the shape of initial distribution of nucleons in momentum space may be changed and energetic nucleons may escape out of the nuclei [41]. Therefore, the average kinetic energy of nucleons in the reaction system decreases and then cause less π^+ meson or hard photon productions. The increased stability of colliding nuclei may cause somewhat more π^+ meson or hard photon productions (less emission of high-momentum nucleons corresponds to a higher average kinetic energy of nucleons in nuclei). Thus considering stability of colliding nuclei, more pion and hard photon may be produced than that in the present work. In a word, after considering stability of colliding nuclei and comparing to the same experimental data, the high-momentum cutoff parameter λ should be smaller than our current constraint. Also uncertainty of the mechanism of hard photon productions may affect the conclusion here. The probability of hard photon production from the semiclassical hard sphere collision model [31, 47, 48] will give somewhat more photon production [28], thus also require a smaller λ value to explain the experimental data. Furthermore, the off-shell transport of particle production in the BUU model may also cause more π^+ meson and hard photon productions [65–67], thus also require a smaller λ value to fit the experimental data. As in this work the λ value is

constrained to be $\lambda \leq 2$, while considering all the above factors, the λ parameter should be not larger than 2.

In conclusions, based on the nuclear transport model, we studied how the high-momentum cutoff parameter λ affects π and hard photon productions in nucleus-nucleus collisions at intermediate energies. It is found that π^+ and hard photon productions in nucleus-nucleus collision at lower beam energy is very sensitive to the value of the high-momentum cutoff parameter λ. By comparing the BUU's π^+ and hard photon productions with experimental data and considering some uncertainties, a constraint of high-momentum cutoff value $\lambda \leq 2$ is obtained.

Constraints on the high-momentum cutoff parameter λ in nuclei have implications in the studies of nuclear force at short distance, in the construction of nuclear transport model of heavy-ion collisions at intermediate energies, in the studies of equation of state of dense nuclear matter and the nuclear symmetry energy at suprasaturation densities or in the study of the physics in neutron stars, etc.

The work was carried out at National Supercomputer Center in Tianjin, and the calculations were performed on TianHe-1A. The work is supported by the National Natural Science Foundation of China under Grant Nos. 11375239, 11435014.

[1] L. Lapikas, Nucl. Phys. A. **553**, 297 (1993).
[2] J. Kelly, Adv. Nucl. Phys. **23**, 75 (1996).
[3] R. Subedi et al. (Hall A. Collaboration), Science **320**, 1476 (2008).
[4] E. Piasetzky, M. Sargsian, L. Frankfurt, M. Strikman, J. W. Watson, Phys. Rev. Lett. **97**, 162504 (2006).
[5] R. Shneor et al., Phys. Rev. Lett. **99**, 072501 (2007).
[6] M. M. Sargsian, T. V. Abrahamyan, M. I. Strikman and L. L. Frankfurt, Phys. Rev. C **71**, 044615 (2005).
[7] R. Schiavilla, R. B. Wiringa, S. C. Pieper and J. Carlson, Phys. Rev. Lett. **98**, 132501 (2007).
[8] H. A. Bethe, Ann. Rev. Nucl. Part. Sci. **21**, 93 (1971).
[9] A. N. Antonov, P. E. Hodgson and I. Z. Petkov, *Nucleon Momentum and Density Distributions in Nuclei* (Clarendon Press, Oxford, 1988).
[10] A. Rios, A. Polls, and W. H. Dickhoff, Phys. Rev. C **79**, 064308 (2009).
[11] P. Yin, J. Y. Li, P. Wang, and W. Zuo, Phys. Rev. C **87**, 014314 (2013).
[12] Claudio Ciofi degli Atti, Physics Reports **590**, 1 (2015).
[13] C. Ciofi degli Atti, S. Simula, Phys. Rev. C **53**, 1689 (1996).
[14] S. Fantoni and V. R. Pandharipande, Nucl. Phys. A **427**, 473 (1984).
[15] S. C. Pieper, R. B.Wiringa, and V. R. Pandharipande, Phys. Rev. C **46**, 1741 (1992).
[16] K. Sh. Egiyan, et al., Phys. Rev. C **68**, 014313 (2003).
[17] O. Hen, L. B. Weinstein, E. Piasetzky, G. A. Miller, M. M. Sargsian, and Y. Sagi, Phys. Rev. C **92**, 045205 (2015)
[18] O. Hen, B. A. Li, W. J. Guo, L. B. Weinstein, and E. Piasetzky, Phys. Rev. C **91**, 025803 (2015).
[19] B. J. Cai, B. A. Li, Phys. Rev. C **92**, 011601 (2015).
[20] O. Hen et al. (The CLAS Collaboration), Science **346**, 614 (2014).
[21] K. S. Egiyan, et al., Phys. Rev. Lett. **96**, 082501 (2006).
[22] M. McGauley and Misak M. Sargsian, arXiv: 1102.3973v3 (2012).
[23] P. Wang, S.-X. Gan, P. Yin and W. Zuo, Phys. Rev. C **87**, 014328 (2013).
[24] F. Zhang, G. C. Yong, arXiv: 1605.03656 (2016).
[25] "Topical issue on nuclear symmetry energy", Eds., B. A. Li, A. Ramos, G. Verde, and I. Vidaña, Eur. Phys. J. A **50**, No. 2, (2014).
[26] Jan Ryckebusch, Wim Cosyn, Maarten Vanhalst, Phys. Rev. C **83**, 054601 (2011).
[27] R. Stock, Phys. Rep., **135**, 259 (1986).
[28] G. C. Yong, B. A. Li, and L. W. Chen, Phys. Lett. B **661**, 82 (2008).
[29] G. C. Yong, W. Zuo, and X. C. Zhang, Phys. Lett. B **705**, 240 (2011).
[30] H. Xue, C. Xu, G. C. Yong, Z. Z. Ren, Phys. Lett. B **755**, 486 (2016).
[31] G. F. Bertsch and S. Das Gupta, Phys. Rep. **160**, 189 (1988).
[32] P. Danielewicz, R. Lacey, W. G. Lynch, Science **298**, 1592 (2002).
[33] D. Persram and C. Gale, Phys. Rev. C **65**, 064611 (2002).
[34] Misak M. Sargsian, Phys. Rev. C **89**, 034305 (2014).
[35] C. Xu, A. Li, B. A. Li, J. of Phys: Conference Series **420**, 012090 (2013).
[36] C. B. Das, S. DasGupta, C. Gale, B. A. Li, Phys. Rev. C **67**, 034611 (2003).
[37] J. Xu, L. W. Chen, B. A. Li, Phys. Rev. C **91**, 014611 (2015).
[38] Isaac Vidana, Artur Polls, Constanca Providencia, Phys. Rev. C **84**, 062801 (R) (2011).
[39] A. E. L. Dieperink, Y. Dewulf, D. VanNeck, M. Waroquier, V. Rodin, Phys. Rev. C **68**, 064307 (2003).
[40] T. Song, and C. M. Ko, Phys. Rev. C **91**, 014901 (2015).
[41] G. C. Yong, Phys. Rev. C **93**, 044610 (2016).
[42] B. A. Li, G. C. Yong, W. Zuo, Phys. Rev. C **71**, 014608 (2005).
[43] N. Gan et al., Phys. Rev. C **49**, 298 (1994).
[44] W. Bauer, G.F. Bertsch, W. Cassing and U. Mosel, Phys. Rev. C **34**, 2127 (1986).
[45] W. Reisdorf et al., Nucl. Phys. A **848**, 366 (2010).
[46] E. Grosse et al., Europhys. Lett. **2**, 9 (1986).
[47] H. Nifenecker and J.A. Pinston, Annu. Rev. Nucl. Part. Sci., **40**, 113 (1990).
[48] W. Cassing, V. Metag, U. Mosel, and K. Niita, Phys. Rep. **188**, 363 (1990).
[49] Y. Schutz et al. for the TAPS collaboration, Nucl. Phys. A **622**, 404 (1997).
[50] G. Martinez et al., Phys. Lett. B **461**, 28 (1999).
[51] David d'Enterria et al., Phys. Lett. B **538**, 27 (2002).
[52] R. Ortega et al., Eur. Phys. J. A **28**, 161 (2006).
[53] G. H. Liu et al., Phys. Lett. B **663**, 312 (2008).
[54] Y. G. Ma et al., Phys. Rev. C **85**, 024618 (2012).
[55] B. A. Remington, M. Blann and G. F. Bertsch, Phys. Rev. Lett. **57**, 2909 (1986).

[56] C. M. Ko, G. F. Bertsch and J. Aichelin, Phys. Rev. C **31**, 2324(R) (1985).
[57] W. Cassing, T. Biro, U. Mosel, M. Tohyama, and W. Bauer, Phys. Lett. B **181**, 217 (1986).
[58] J. Stevenson et al., Phys. Rev. Lett. **57**, 555 (1986).
[59] C. M. Ko and J. Aichelin, Phys. Rev. C **35**, 1976 (1987).
[60] H. Nifenecker and J. P. Bondorf, Nucl. Phys. A **442**, 478 (1985).
[61] K. Nakayama and G. F. Bertsch, Phys. Rev. C **34**, 2190 (1986).
[62] M. Schäffer, T.S. Biro, W. cassing and U. Mosel, H. Nifenecker and J.A. Pinstan, Z. Phys. A **339**, 391 (1991).
[63] R. G. E. Timmermans, T. D. Penninga, B. F. Gibson, M. K. Liou, Phys. Rev. C **73**, 034006 (2006).
[64] Y. Safkan et al., Phys. Rev. C **75**, 031001(R) (2007).
[65] G. F. Bertsch, P. Danielewicz, Phys. Lett. B **367**, 55 (1996).
[66] W. Cassing and S. Juchem, Nucl. Phys. A **665**, 377 (2000).
[67] A. B. Larionov and U. Mosel, Phys. Rev. C **66**, 034902 (2002).